Korean J. Chem. Eng., 39(6), 1604-1613 (2022)
DOI: 10.1007/s11814-021-1010-2

pISSN: 0256-1115
eISSN: 1975-7220

In situ soft templated synthesis of polyfluorene-molybdenum oxide (PF-MoO_3) nanocomposite: A nanostructure glucose sensor

Bhagyashri Bajirao Kamble*, Paurnima Talele, Anita Kundlik Tawade***, Kirankumar Kakchingtabam Sharma***, Sawanta Subhash Mali****, Chang Kook Hong****, and Shivaji Nemchand Tayade*,†**

*Department of Chemistry, Shivaji University, Kolhapur-416004, Maharashtra, India
**Department of Chemistry, Indian Institute of Technology Madras, Chennai-600036, India
***School of Nanoscience and Technology, Shivaji University, Kolhapur-416004, Maharashtra, India
****Polymer Energy Materials Laboratory, School of Advance Chemical Engineering, Chonnam National University 61186, Korea
(*Received 20 August 2021 • Revised 8 November 2021 • Accepted 10 November 2021*)

Abstract−A polyfluorene-molybdenum oxide nanocomposite (PF-MoO_3) was successfully prepared in swollen liquid crystalline (SLC) lamellar phase. The morphology, shape, and structure of the nanocomposite are characterized by field emission scanning electron microscopy (FESEM), X-ray powder diffraction (XRD), and Fourier transform infrared spectroscopy (FTIR). The obtained PF-MoO_3 material was loaded over a glassy carbon electrode (GCE). The PF-MoO_3/GCE was employed as a working electrode for the detection of glucose by differential pulse voltammetry (DPV) and cyclic voltammetry (CV) techniques. The determined limits of detection (LOD) and the limits of quantification (LOQ) from CV were 7.90×10^{-5} M and 2.63×10^{-5} M, respectively. The calculated sensitivity of the PF-MoO_3 electrode material for glucose was estimated to be 4.29×10^{4} μA L mol^{-1} cm^{-2}. The values of LOD and LOQ obtained from DPV data were 7.05×10^{-5} M and 2.35×10^{-5} M, respectively. The results were in agreement with CV observations. Similarly, the glucose sensitivity for the PF-MoO_3/GCE by DPV technique was 5.18×10^{3} μA L mol^{-1} cm^{-2}. In this research, we have developed a highly sensitive glucose sensor by modification of the GCE electrode surface with PF-MoO_3 nanocomposite.

Keywords: Nanocomposite, Swollen Liquid Crystal, Hydrothermal, Conducting Polymer, Glucose Sensor

INTRODUCTION

In healthy human blood, the normal concentration of glucose is around 72 mg/dL, but any drastic change in sugar level leads to diabetes and kidney disease [1]. Nowadays, diabetes is the foremost health care challenge, and approximately 171 million people across the globe are suffering from it. Testing glucose levels is especially important for diabetic patients to avoid complications. Most diabetic patients are accustomed to dealing with blood sugar checks as part of their daily routine. Therefore, considering healthcare awareness, the area of glucose sensors is identified as a top priority among researchers.

Enzymatic glucose biosensors have been developed for a long time. The most common and serious problem with these enzymatic sensors is their lack of stability arising due to the nature of enzymes. To overcome this issue, nonenzymatic glucose sensors have been explored [2]. Despite significant dedicated efforts towards the development of non-enzymatic nanomaterials-based electrodes for accurate sensing of glucose, there are some drawbacks. Typically, inert (noble) metals such as platinum (Pt), gold (Au), and palladium (Pd) based nanomaterials or composites are reported as non-enzymatic glucose sensors by using different electrochemical approaches like CV and DPV [3,4]. However, these noble metals are costly and have limited formation of a homogeneous dispersion, which is directly impacting the cost and reproducibility [5,6]. Therefore it is important to investigate low-cost and enzyme-free glucose sensors. Transition metal dichalcogenides (WS_2, MoS_2, and WSe_2) [7,8], transition metal oxide (TiO_2, CuO) [9,10], and polymer-metal composite [11,12] can be used for electrochemical sensing of glucose. Among various transition metal dichalcogenides, MoS_2 has been widely explored and believed to be a potential candidate in electrochemical sensing towards glucose due to its chemical inertness, unique atomic structure (sheet-like), and high surface area. However, MoS_2 has shown poor electrochemical performance due to low electrical conductivity and restacking sheet structure, which reduces the rate of charge transfer reaction and active reaction sites. Whereas molybdenum-based oxide (MoO_3) has prominent features, such as a unique structure composed of octahedron MoO_6 layers and connected by weak van der Waals force consisting of the gap between the layers (around 2.6 Å) [13]. These distinctive structural aspects of MoO_3 expedite the intercalation of glucose analyte, and considerable redox behavior of MoO_3 would improve the electrode/electrolyte interface area [14]. Therefore, MoO_3 is substantially utilized for electrochemical sensing of biomolecules such as dopamine. It has been reported that bonding between Mo-O in MoO_3 facilitates electrocatalytic oxidation of dopamine [15]. Bonding character and unique structural features make MoO_3 an excellent candidate for electrochemical sensing applications. The

†To whom correspondence should be addressed.
E-mail: snt_chem@unishivaji.ac.in

rise of conducting polymers like polyaniline, polypyrrole, and polyfluorene (PANI, PPY, and PF) can give a new prospect for the production of hybrid composites having high thermal, chemical stability with good conductivity [16-18]. Conducting polymers and metal oxide nano-composites are anticipated to be a vital example of materials in various fields such as electronics, [19] energy storage [20], and sensing [21]. The combination of polymer and metal oxide has been applied in various fields, such as conducting PANI-ZnO coating as a high corrosion resistance [22] and conducting PANI-MoO_3 hybrid nanomaterials for supercapacitor [23]. These studies have suggested that doping of conducting polymers with transition metal oxide increases the charge delocalization in the conducting polymer backbone, leading to higher conductivity [24]. The association of MoO_3 with redox-active conducting polymers is an excellent way to enhance the electro-catalytic properties and stability. Among various polymers, polyfluorene (PF) possesses planar biphenyl units with high π bond conjugation and good electrical conductivity [25]. Hence, polyfluorene has drawn considerable attention in mechanical properties [26,27].

A stable and sensitive electrode material for selective glucose-sensing can be obtained through the combination of PF and MoO_3. Surfactant-based swollen liquid crystalline (SLC) mesophase is well known soft template nanoreactor for the synthesis of conducting polymers and different metal nanostructures. We have recently demonstrated this method for synthesizing multifunctional PANI-Pd composite [28] and hybrid nanocomposite PANI-ZnO-GO for pesticide detection [29]. In the current study, we prepared PF-MoO_3 nanocomposites in SLC. The morphology, shape, and structure of nanocomposites were characterized by field emission scanning electron microscopy (FESEM), X-ray powder diffraction (XRD) and Fourier transform infrared spectroscopy (FT-IR), respectively. Cyclic voltammetry (CV) and differential pulse voltammetry (DPV) were used to evaluate the electrochemical performance of PF-MoO_3 nanocomposites modified electrode towards glucose. Here we have successfully developed PF-MoO_3 nanocomposite electrode material as a non-enzymatic glucose sensor.

EXPERIMENTAL

1. Reagents

Ethyl alcohol (C_2H_5OH, 99%), concentrated nitric acid (HNO_3, 99.0%), ammonium heptamolybdate tetrahydrate (AHM, $(NH_4)_6Mo_7O_{24}\cdot 4H_2O$, 99.0%) cetyl-pyridinium chloride monohydrate ($CPCl\cdot H_2O$, 99.0%), cyclohexane (C_6H_{12}, 99%), 1-pentanol ($C_5H_{12}O$, 99.0%), potassium permanganate ($KMnO_4$, 99.0%), glacial acetic acid (CH_3COOH, 99.0%), sodium acetate (CH_3COONa, 99.0%), isopropyl alcohol ($CH_3CHOHCH_3$, 99.0%) of the best available purity grade were purchased from Thomas Baker Pvt. Ltd., India. Fluorine monomer was procured from Sigma-Aldrich Chemical Company, USA. The values in the parentheses are purities of these substances as stated by the vendor. The water used to prepare solutions was triple distilled. All the reagents were of A.R grade and utilized with no further purification.

2. Synthesis of MoO_3 by Facile Hydrothermal Method

We used hydrothermal method with slight modification for the synthesis of MoO_3 [30]. Aqueous solution of AHM (0.05 M) was prepared and stirred for 10 minutes. The concentrated HNO_3 was added dropwise into aqueous AHM solution with continuous stirring. 20 mL of the acidic AHM solution was added to a Teflon lined stainless steel autoclave (capacity 50 ml). The reaction was done in a muffle oven for 8 hrs at 180 °C. The resulting product was subsequently separated via centrifugation and cleaned with deionized water and ethanol, respectively. Later, MoO_3 was dried at 60 °C and annealed at 350 °C.

The overall reaction mechanism of MoO_3 as per reported literature [30] is depicted in reaction Eqs. (i)-(ii).

$$(NH_4)_6Mo_7O_{24}\cdot 4H_2O+6HNO_3\rightarrow H_6Mo_7O_{24}\cdot 4H_2O+6NH_4NO_{3(aq)} \quad (i)$$

$$H_6Mo_7O_{24}\cdot 4H_2O\rightarrow 7MoO_3+7H_2O \quad (ii)$$

According to the above reaction equations, initially, acidified precursor (AHM) gets converted into intermediate species depicted in (i), which is further later dehydrated into a final product of MoO_3 shown in reaction Eq. (ii).

3. Synthesis of PF-MoO_3 Composite in Swollen Liquid Crystalline Lamellar Mesophase

Synthesized MoO_3 was further used for in situ preparation of PF-MoO_3 nanocomposite by swollen liquid-crystalline method (SLC) [29]. Initially, the fluorene monomer was dissolved in ether (0.1 mol L^{-1}). The dissolved monomer was introduced into a 30-ml glass tube and mixed with cetylpyridinium chloride (CPCl). This was followed by the addition of 2 ml of water, which resulted in a viscous and turbid solution. Sequentially, cyclohexane (3 ml) was added to the prepared mixture and vigorously vortexed to yield lamellar mesophase. Co-surfactant 1-pentanol (350 μL) was added to the mixture by strong vortexing for 2 min and previously dispersed MoO_3 in ethanol (1 mg/ml) was added to the above mixture. At this stage, the formation of lamellar mesophase took place. To this transparent lamellar mesophase, $KMnO_4$ (0.01 M) was added as initiator and then the whole system was placed at the darkroom temperature. Primarily, the mesophase transformed to a dark brown, and then the entire system was kept for the chain polymerization process for 24 hours. The composite materials were washed several times with isopropyl alcohol followed by water. The brown-colored product was dried in the oven at 60 °C for 12 hrs. Fig. 1 shows the overall schematic presentation of the experimental procedure.

4. Active Surface Area of PF-MoO_3/GCE Electrode

The active surface area of the modified electrode was calculated using Randles-Ševcik equation for a reversible redox process [59]. 1 mM ferrocene was used as a standard redox couple in 0.1 M KCl.

$$i_p=(2.69\times 10^5)(n)^{3/2}\,AD_{app}^{1/2}C_o\upsilon^{1/2} \quad (1)$$

where, 'i_p' represents the oxidative peak current (anodic), 'n' is number of electrons involved in the electrode reaction=1, 'A' is the surface area of the electrode, 'D_{app}' is the diffusion coefficient=0.16×10^{-6} cm^2 s^{-1} [31]. 'υ' is the scan rate (V s^{-1}). The concentration of ferrocene (1 mM) is denoted by 'C_o'. The active surface area of the modified electrode was (0.54 cm^2), which is eight-times greater than the geometric area (0.07 cm^2) of bare GCE. The calculated roughness factor was found to be 7.73.

5. Instrumentation

The diffraction spectra were recorded at the angle of 5^0 to 90^0

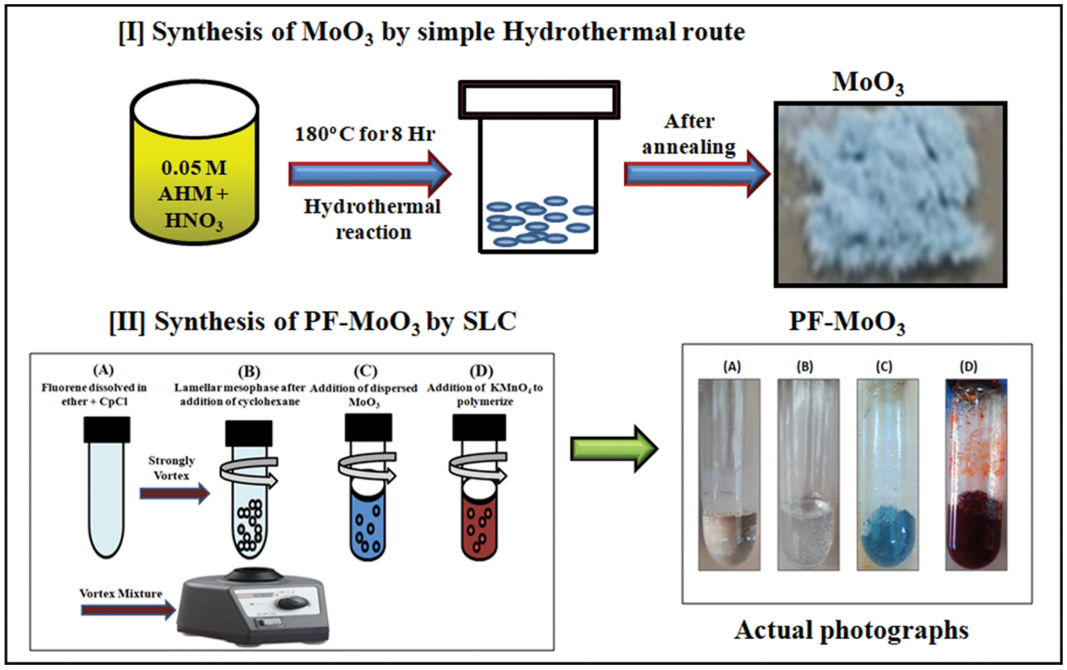

Fig. 1. Schematic illustration of the hydrothermal synthesis of MoO_3 and synthesis of PF-MoO_3 nanocomposite by SLC.

using XRD (Thermo ARL X'TRA with CuKα λ=0.154 nm). The crystalline characteristics of the PF-MoO_3, crystalline size, and structural parameters were determined. Functional group studies were done using Fourier transform infrared spectroscopy (FT-IR Spectrometer 4600, Jasco) using KBr pellets. The morphology of the PF-MoO_3 composite was investigated by field emission scanning electron microscopy (FE-SEM). (Nova nanosem 450). Three electrode systems PGSTAT 302 N Autolab Metrohm were used for the electrochemical performance study.

RESULTS AND DISCUSSION

1. Structural Studies

Crystalline performance of synthesized PF, MoO_3, and PF-MoO_3 is depicted in Fig. 2. The typically developed diffractogram of MoO_3 thin film is represented in Fig. 2(a). Every peak was well indexed to hexagonal MoO_3 [JCPDS card (21-0569)] [32]. Sharp and highly intense peaks demonstrate the fine crystallinity of hexagonal MoO_3. Fig. 2(b) shows the slightly thin peak at 9° and wide peaks between 10° and 30° (2θ) which are the characteristic peaks of polyfluorene due to the presence of polymeric chain. This observation confirms the presence of polyfluorene in the semi-crystalline phase and the results are consistent with earlier reports [33-35]. Fig. 2(c) shows the XRD pattern of the PF-MoO_3 composite. The disappearance of crystalline peaks with the incorporation of polyfluorene to MoO_3 indicates modification of MoO_3 with PF results in enhancing the amorphous nature in PF-MoO_3 composite. This is attributed to the subsistence of polyfluorene. The existence of broad peaks in Fig. 2(c) is ascribed to the stacking phase of polymers caused by the stacking of aromatic main chains [36]. Additionally, the disappearance of XRD peaks (2θ=25°) of MoO_3 suggests that the low concentration of molybdenum influences the overall crystal features of the PF-MoO_3 composite. The mean crystallite sizes of MoO_3 and PF-MoO_3 were calculated by Scherrer's eq and it was found to be 90 nm and 27.37 nm, respectively.

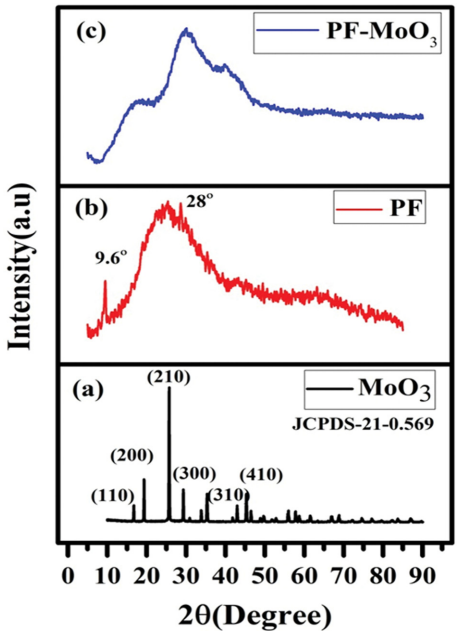

Fig. 2. X-ray diffraction patterns (a) MoO_3, (b) PF and (c) PF-MoO_3 composite.

2. Morphological Analysis (FE-SEM)

Morphological and structural analysis of PF-MoO_3 composite was carried out by field emission scanning electron microscopy (FE-SEM). In Fig. 3, (a) and (b) are FE-SEM images for synthesized MoO_3 while (c) and (d) are for PF-MoO_3 composite. It is

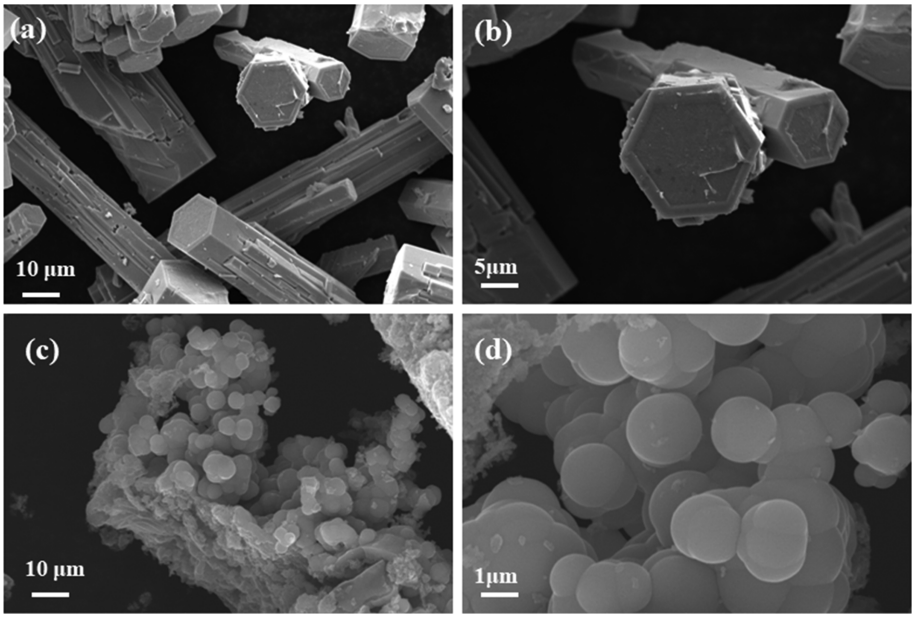

Fig. 3. FESEM images of MoO_3 (a) and (b); PF-MoO_3 composite (c) and (d).

seen from FE-SEM images that MoO_3 is in the hexagonal rod shape morphology and PF-MoO_3 composite represents sphere shape morphology. The discrepancy in the morphology is due to the association of polymer matrix with metal oxides. The morphology of composite is influenced by polymer matrix by their properties like surface functionalization and stabilizer. From the FE-SEM analysis, it was confirmed that microspheres of polyfluorene were effectively encapsulated all over the surface of MoO_3. As a result, the surface became rough, indicating the efficient coating of polymers at the surface of MoO_3 [37,38] and, consequently, the hexagonal morphology of MoO_3 vanished. The disappearance of the hexagonal shape of MoO_3 is due to the modification of metal surfaces with appropriate polymers via strong steric interaction [39]. Increasing the concentration of polyfluorene in the composites leads to reducing the hexagonal shape of MoO_3 in the composite. Thus, it is predictable that PF-MoO_3 can exhibit superior sensitivity towards glucose due to the presence of a rough surface which offers more active sites for the immobilization of glucose analyte.

3. Functional Group Studies (FT-IR)

FT-IR spectra provide the details of functions groups and confirm the complexation and interaction among the compounds. Fig. 4(a) shows the FT-IR spectrum of MoO_3 with the resultant absorption band occurring at 521 cm^{-1} and 646 cm^{-1} that are related to the vibration of Mo-O bond; peaks at 913 cm^{-1} and 974 cm^{-1} are characteristic vibration bands of Mo=O in hexagonal phase, while vibration detected at 1,402 cm^{-1} was associated with the vibration mode of the Mo-OH bond. Absorption peaks at 1,689 cm^{-1} and 3,550 cm^{-1} are allied with bending and stretching vibration of hydroxyl (-OH) group of water molecule [40]. The absorption peaks in the region of 1,000-400 cm^{-1} suggest the inter-atomic vibration of metal and oxygen. Fig. 4(b) describes the FT-IR spectra of PF with chain C-H stretching at 2,846 cm^{-1}. The band at 2,924 cm^{-1}

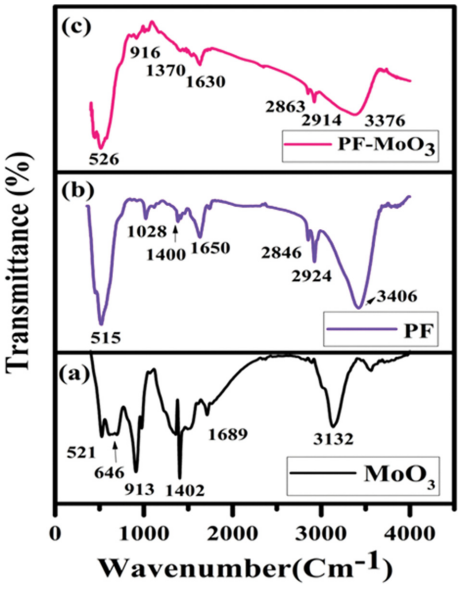

Fig. 4. FT-IR spectrum (a) MoO_3, (b) PF, (c) PF-MoO_3.

confirms the aromatic C-H stretching. The absorption bands 1,400 cm^{-1} and 1,650 cm^{-1} are a sign of the presence of aromatic ring vibration and C=C stretching frequency. The stretching and bending vibrations in PF-MoO_3 composite are depicted in Fig. 4(c). The fingerprint region peaks at 526 cm^{-1} and 916 are attributed to Mo-O and M=O bond stretching frequency [40]. Vibrations observed at 1,370 cm^{-1} and 1,630 cm^{-1} confirm the conjugation upon a combination of polyfluorene to MoO_3. A spacious band at 3,376 cm^{-1} corresponds to the stretching frequency of the OH- group. The bands at 2,863 cm^{-1} and 2,914 cm^{-1} are characteristic of the C-H stretching (alkyl chain) and C-H stretching of the aromatic ring of polyfluorene, respectively [41]. These results of the FT-IR

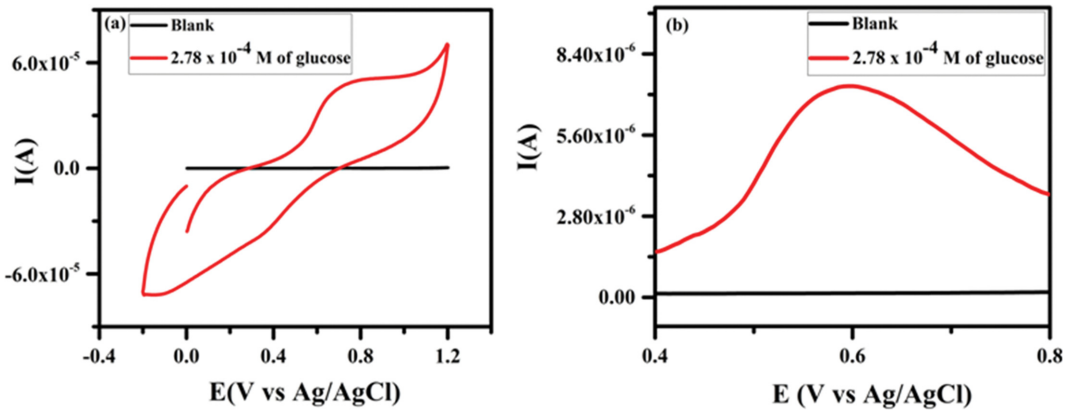

Fig. 5. Voltammogram of glucose (0.1 M acetate buffer; pH 7.4) at the PF-MoO_3/GCE (a) CV of 2.78×10^{-4} M glucose (b) DPV of 2.78×10^{-4} M glucose.

spectrum confirm the successful formation of composite and strong interaction of PF and MoO_3 particles.

4. Electrochemical Activity of Glucose at PF-MoO_3/GCE

The voltammetric response of glucose (2.78×10^{-4} M) was investigated in 0.1 M acetate buffer (pH 7.4). Fig. 5(a) and 5(b) depict CV and DPV in the presence and absence of glucose (blank solution) over the surface of PF-MoO_3/GCE at optimum conditions. It is clearly evident from Fig. 5(a) that no Faradic response was recorded in the blank solution. In the presence of glucose, the forward scan shows single broad, plateau-shaped peak at E_{ox}=0.75 V signaling the oxidation of glucose (anodic peak). The reverse scan shows the corresponding reduction peak at E_{red}=0.38 V (cathodic peak). This implies that the modified PF-MoO_3/GCE is highly sensible towards glucose. The redox behavior of glucose is found to be quasi-reversible, as can be seen peak separation of 370 mV in the oxidation and reduction peak positions. Similarly, in Fig. 5(b) DPV of glucose (2.78×10^{-4} M) exhibits a broad oxidation peak at 0.6 V due to the significant electro-catalytic activity of glucose at the surface of PF-MoO_3/GCE. While in the absence of glucose no redox response is recorded. In the forward scan (0 to 1.2 V), the molybdenum metal is in (VI) state. This electron-deficient state catches up the electrons from glucose to produce gluconolactone. During this process, Mo (VI) is reduced to Mo (V) in the form of PF-MoO_2 (OH^-) [42]. The possible reaction mechanism is according to the following reaction equation:

$$\text{PF-MoO}_3+\text{Glucose}\rightarrow\text{PF-MoO}_2\,(\text{OH})^-+\text{Gluconolactone}$$

Fig. 6 shows a general representation of the electron transfer process involved in glucose oxidation.

5. Effect of Glucose Concentration on the CV and DPV

CV and DPV method were employed to study the influence of glucose concentration at the surface of PF-MoO_3/GCE at the optimized conditions. Fig. 7(a) shows CV of rise in concentration of glucose ranges from 1.39×10^{-4} M to 9.72×10^{-4} M. The anodic peak current increases linearly with respect to increasing glucose concentration. The oxidation peak potential is allied with the low to high concentration (0.75 to 0.76 V). The negligible shifting in peak potential signifies the rapid electron transfer of glucose over the surface of PF-MoO_3/GCE. Fig. 7(b) portrays the linear correlation

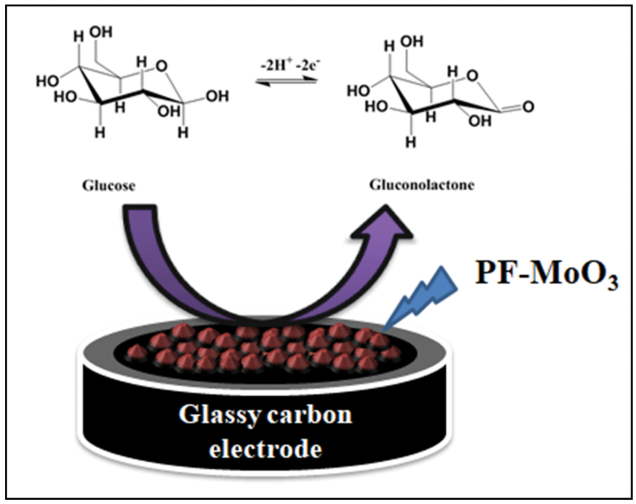

Fig. 6. Electron transfer process of glucose at surface of PF-MoO_3/GCE.

in oxidation peak current and concentration of glucose. The linear regression Eq. (2) is as follows:

$$I_a(A)=0.0232\ C+2.0\times10^{-5}(A)\ (R^2=0.9936) \quad (2)$$

Fig. 7(c) depicts DPV of glucose concentration varies from 2.77×10^{-4} to 9.72×10^{-4} M under optimum conditions. Fig. 5(c) decodes that the anodic peak current was increased with an increase in glucose concentration, while Fig. 7(d) shows the linearity between anodic peak current against concentration of glucose. The linear regression Eq. (3) is given by

$$i_p(A)=0.0028C+5.0\times10^{-6}(A)\ (R^2=0.9934) \quad (3)$$

CV and DPV are sensitive tools towards electrochemical analysis and to give significant information about lowest concentration of an analyte. Therefore, from the calibration curve of CV and DPV, the detection limits were calculated by using Eqs. (4) and (5), respectively [43]. LOD were found as 7.90×10^{-5} M, and 7.05×10^{-5} M and LOQ were calculated 2.63×10^{-5} M and 2.35×10^{-5} M:

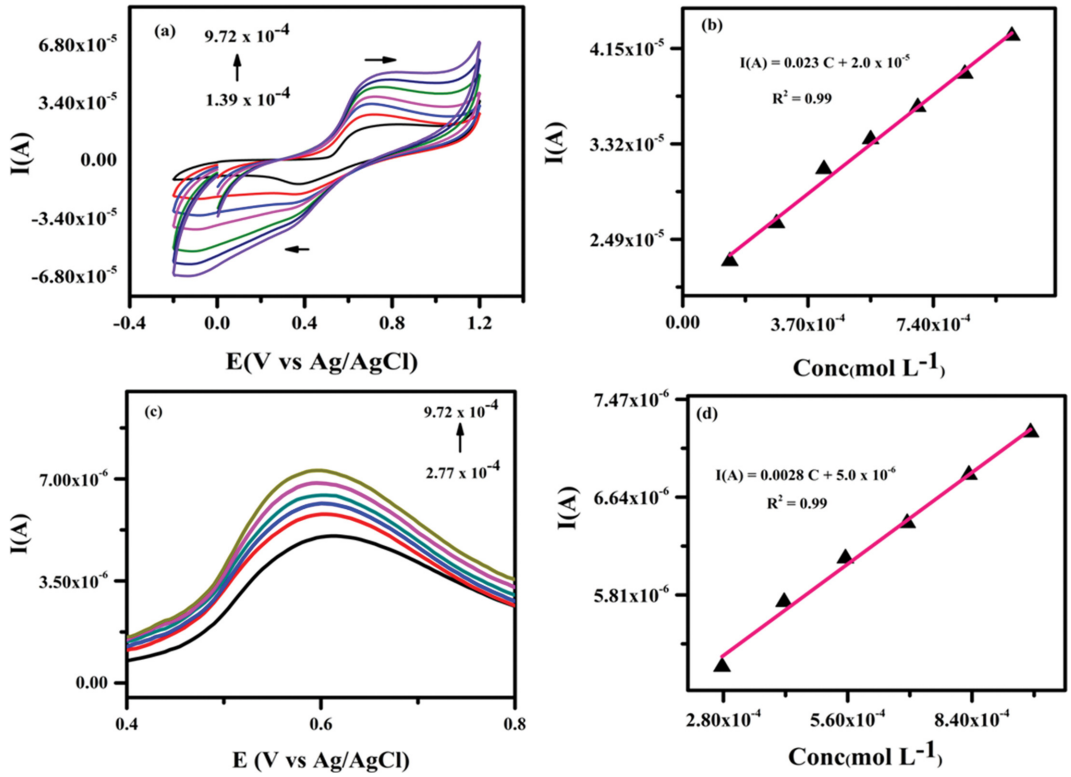

Fig. 7. (a) Effect of glucose concentration (CV) (1.39×10^{-4} M to 9.72×10^{-4} M) at the PF-MoO_3/GCE (acetate buffer of 0.1 M, pH 7.4) at scan rate 50 mV/s. (b) The linearity of oxidation peak current with respect to the increasing concentration of glucose. (c) DPV of various concentration of glucose (2.77×10^{-4}-9.72×10^{-4} M) at PF-MoO_3/GCE (acetate buffer of 0.1 M; pH 7.4) with the scan rate 50 mV/s. (d) The linear variation of oxidation peak current against the concentration of glucose.

Table 1. Comparative study of glucose oxidation potential at various electrode materials

Sr No	Electrode material for glucose sensing	Potential (V)	Ref.
1	Au/Fe_2O_3	0.9	52
2	$ZnFe_2O_4$/PPy	0.9	53
3	SWCNT/GOx/Nafion composite	0.8	54
4	NiNPs/PEDOT/RGO	0.5	55
5	RuOx-Prussian Blue/GCE	1.10	56
6	**PF-MoO_3/GCE**	**0.75 (CV)**	**Present work**
7	**PF-MoO_3/GCE**	**0.60 (DPV)**	**Present work**

$$LOD=3\sigma/M \quad (4)$$

$$LOQ=10\sigma/M \quad (5)$$

where, σ signifies the standard deviation (obtained from anodic peak current) and M represents the slope (from calibration curve) (Fig. 7(b) and Fig. 7(d)). Table S1 provides comparative performance of the PF-MoO_3/GCE with other molybdenum based modified electrode; from the comparison it is clear that PF-MoO_3/GCE possesses remarkable sensitivity towards glucose and even better detection limit than some of the modified electrodes [44,47,50]. Few molybdenum based materials (MoS_2) [45,46,49,51] have better performance than PF-MoO_3 but require doping of expensive noble metals (Ag, and Pd) and mix metals, which involves sensitive synthesis route. Herein, we have developed simple surfactant-based synthesis of PF-MoO_3, which involves in situ polymerization at room temperature. Table S1 represents the designed sensor PF-MoO_3 with wide linear range compared to the other reported modifiers. The sensitivity of the electrode is analogous to the literature.

Table 1 represents a comparison of obtained oxidation potential signals for glucose at different electrodes. This work describes low cost, versatile synthesis tactics for highly sensitive electrode materials for glucose at the lower oxidation potential. The synergetic influences between the PF and MoO_3 module enhanced catalytic activity for detection of glucose at lower energy.

6. Influence of Electrolyte pH

Fig. 8(a) shows redox behavior of glucose (9.72×10^{-4} M) with PF-MoO_3/GCE in 0.1 M acetate buffer of different pH (pH 3.6, 4.9, 9.0 and 7.4) at scan rate 50 mVs^{-1}. From Fig. 8(a) it is quite

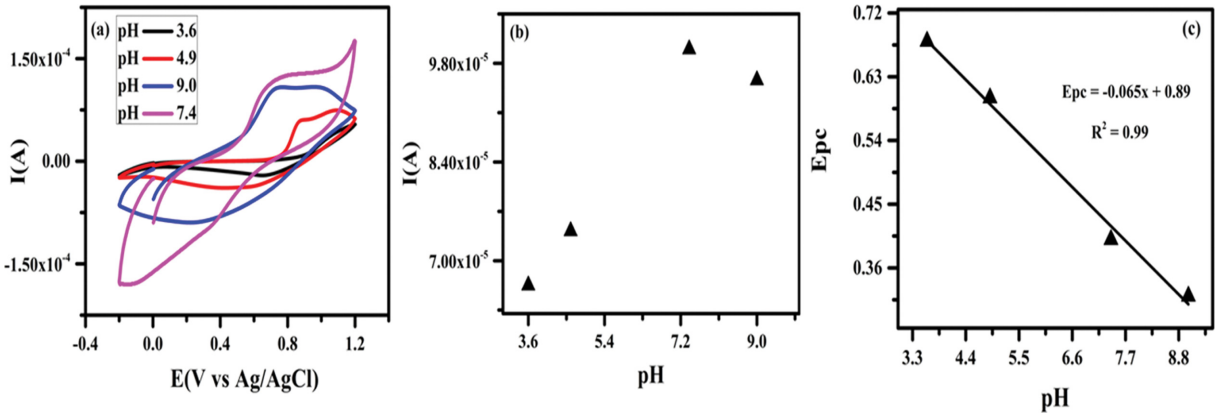

Fig. 8. (a) Obtained CV of glucose (9.72×10^{-4}) M with PF-MoO_3/GCE (acetate buffer of 0.1 M; pH 7.4) at 50 mVs^{-1}. (b) The plot of anodic peak current against different pH. (c) The plot of Epc against different pH.

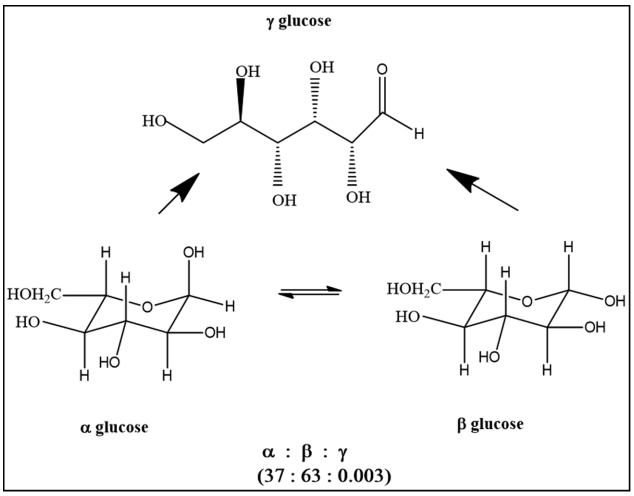

Fig. 9. Stable isomeric form of glucose at equilibrium state.

clear that there is no Faradic activity in pH 3.4, while pH 4.9 and 9 show some redox activity. However, drastic change in the redox peak current was achieved at only pH 7.4. This implies that pH 7.4 is energetically favorable for glucose sensing. Glucose has been more extensively studied in neutral media (pH 7.4) than basic or acidic media, since in neutral media glucose exists in equilibrium state with three isomers α, β, and γ as represented in Fig. 9 [57] [52-55]. In the aqueous solution (pH 7.4), the ratio of $\alpha:\beta:\gamma$ isomers is [37 : 63 : 0.003] at the equilibrium state. A similar ratio is found in the blood as well. The protic environment of solution can shift the ratio of α and β orientation significantly [58]. In basic medium, adsorbed dehydrogenated intermediate gets oxidized to form gluconolactone and slow desorption of gluconolactone takes place along with formation of gluconic acid. In acidic media, glucose is not reactive. Considering the above observation, neutral medium is favorable for glucose oxidation [59].

As is evident, Fig. 8(b) shows a plot of peak current against pH that implies oxidation of glucose is dependent on the pH of an electrolyte. The oxidation peak current of glucose increases as pH value increases, until it reaches a maximum at pH 7.4 and then decreases slowly above pH 7.4, Fig. 8(c) depicts the shifting of Epc towards less positive potential with increasing pH; the linear regression Eq. (6) is as follows:

$$\text{Epc (V)} = -0.065\ \text{pH} + 0.89\ (R^2 = 0.99) \quad (6)$$

where, R^2 is correlation coefficient and the obtained slope −0.065 V/pH is nearly equal to theoretical value 0.059. This result confirms the redox reaction of glucose involves equal number of protons and electrons [60]. From the above experimental observations, pH 7.4 was taken as optimum pH for further electrochemical investigations.

7. Effect of Scan Rate

Dependence of relative change of oxidation and reduction peak current of glucose (9.72×10^{-4} M) with scan rate was studied. Fig. S1(a) shows an overlay CV of glucose and Fig. S1(b) represents a plot of the redox peak current depending on the square root of the scan rate. A linear increase in anodic (oxidation) and cathodic (reduction) peak current was observed with increasing scan rate. However, this was accompanied by slight potential shifting and this shifting of oxidation peak arose due to the disproportion between the Faradic process and mass transport [61]. This effect of scan rate seems to appear as a result of kinetic factors of electrochemical processes at the sensor surface and instrumental circumstances. This behavior indicates that electrode reaction is controlled by a diffusion process [62]. The linear regression equations were found to be with R^2=0.99 (Eqs. (7)-(8)).

$$i_{pa}(10^{-5}\ \text{A}) = 0.00008 + 0.000005\ (\text{V s}^{-1})^{1/2}\ R^2 = 0.99 \quad (7)$$

$$i_{pc}(10^{-5}\ \text{A}) = -0.00006 - 0.000002\ (\text{V s}^{-1})^{1/2}\ R^2 = 0.99 \quad (8)$$

8. Electrochemical Impedance Spectroscopic (EIS) Studies

Electrochemical impedance spectroscopy is a major technique for the elucidation of the charge transfer process at the interface of modified electrode. Fig. S2 shows a Nyquist plot of bare GCE and PF-MoO_3 modified GCE in 0.1 M KCl containing 1 mM ferrocene. A Nyquist plot of bare GCE shows the semicircular region that appears when the charge transfer process is limited between electrode and electrolyte. This indicates a barrier of electron transfer of redox probe at bare GCE. While PF-MoO_3 modified elec-

trode shows a linear region at low frequency, suggesting higher rate of electron transfer process. This observation implies that PF-MoO_3 modified GCE possesses higher conductivity due to the synergic effect of PF and MoO_3. Moreover, the charge transfer resistance (Rct) of bare GCE and PF-MoO_3/GCE was found to be 21.7 Ω, and 1.79 Ω. Low Rct value of PF-MoO_3/GCE shows the high efficiency of PF on MoO_3; therefore, PF-MoO_3 exhibits higher interfacial electron transfer rate.

9. Chronoamperometry Studies

Chronoamperomtery technique was employed to find the number of electrons transferred during glucose oxidation in the optimum condition. It is an extensively used method due to its high sensitivity; here, the Cottrell Eq. (10) was used to derive the number of electrons. From the Cottrell plot of I vs. $t^{-1/2}$, the linear regression equation was found as Eq. (9) (Fig. S3):

$$I(A)=3.0\times10^{-6}-2.0\times10^{-8}\ (R^2=0.99) \tag{9}$$

The obtained slope from the above equation was used in the Cottrell Eq. (10):

$$I(A)=\frac{nFAC^*\ D^{1/2}}{\pi^{1/2}t^{1/2}} \tag{10}$$

where, F is denoted for Faraday constant=96,485 C mol^{-1}, 'A' signifies geometrical area=0.07 cm^2, concentration of ferrocene given by 'C*'=0.5 mM, and the value of D was obtained from literature 8.6×10^{-4} cm^2/s [63]. The calculated number of electrons transferred in glucose oxidation was 1.83~2; this calculated value is consistent with Fig. 6.

10. Reproducibility and Stability

The reproducibility was investigated by four repetitive measurements with unlike PF-MoO_3/GCE. As a result, nearly the matching oxidation peak current was monitored by the CV at optimum conditions and the resultant RSD (relative standard deviation.) value was 2.0%. The stability of the modified GCE was inspected by CV using glucose (2.78×10^{-4} M) in favorable conditions (0.1 M acetate buffer; pH 7.4), for consecutive 25 cycles. The percentage degradation was calculated using the following formula (Eq. (11)) [60]:

$$\text{degradation }\%=\frac{ip_l}{ip_i}\times100 \tag{11}$$

where, ip_l and ip_i signify last and initial anodic peak current, the calculated degradation percentage was 94% of initial current, which implies suitable stability. Therefore, these observations specify that the proposed sensor exhibits outstanding stability and reproducibility.

11. Estimation of the Diffusion Coefficient of Glucose

Diffusion coefficient of glucose (2.78×10^{-4} M) was anticipated using the modified Randles-Ševcik Eq. (12) [59] at the surface of PF-MoO_3/GCE:

$$i_p=(2.99\times10^5)(\alpha n)^{1/2}n^{3/2}AD_{app}^{1/2}C_o\upsilon^{1/2} \tag{12}$$

where, 'C_0' is concentration of electro-active species (mol cm^{-3}), υ is the scan rate (V s^{-1}). Oxidation peak current is denoted by 'i_p' (A), the geometrical area is represented by 'A' (cm^2), 'α' stands for electron transfer coefficient, diffusion coefficient is given by 'D_{app}' (cm^2 s^{-1}). The calculated apparent diffusion coefficient of glucose was 2.51×10^{-7} cm^2 s^{-1}.

12. Interference Study of Biomolecules

Probable interference for the sensing of glucose was studied using several coexisting antibiotic, lipids(fats), amino acid and enzymes like Ampicillin, Cholesterol, L-Cysteine, L-Asparagine etc. Moreover, the biomolecules such as dopamine (DA), ascorbic acid (AA) and uric acid (UA), which are contemporaneous alongside with glucose, were also examined during interference study. A cyclic voltammogram was recorded to investigate the interference test as represented in Fig. S4. The experiment was carried out with succeeding addition of Ampicillin (874 μM), L-Asparagine (375 μM), L-Cysteine (303 μM), Cholesterol (967 μM), DA (40 μM), AA (35 μM) and UA (35 μM) along with the glucose (0.278 mM), in acetate buffer (pH 7.4). The resultant CV shows higher oxidation peak current at relatively low potential for glucose compared to the other biomolecules and interfering group. This implies that the PF-MoO_3/GCE shows good selectivity towards glucose even in presence of common interfering species.

13. Determination of Glucose in Human Urine Sample

The workability of the designed sensor was inspected using a human urine sample of three healthy volunteers. Urine samples of three volunteers were tested for recovery. The analysis was performed by the addition of 0.684 mM, 0.833 mM and 0.972 mM glucose in each sample, respectively, as shown in Fig. S5. The obtained results show an analysis of glucose concentration in human urine samples using anodic peak potential. The obtained voltammogram shows a clear signal of glucose oxidation with good percentage recovery close to 100. The recovery efficiency was calculated using following formula (Eq. (13)) [64]:

$$\text{Recovery }(\%)=\frac{\text{glucose concentration found}}{\text{glucose concentration added}}\times100 \tag{13}$$

The results of this study confirm the accuracy and suitably of the PF-MoO_3/GCE electrode for glucose sensing. The recovery results are represented in Table 2.

14. Chronoamperometry Studies for Stability and Electro-catalytic Activity

The electro-catalytic activity and stability of PF-MoO_3/GCE was

Table 2. Recovery study of glucose at the PF-MoO_3/GCE

Urine sample	Glucose added (M)	Glucose found (M)	Recovery (%)	RSD (%)
I	6.94×10^{-5}	6.80×10^{-5}	97.9	6.3
II	7.80×10^{-5}	7.49×10^{-5}	96.0	5.8
III	7.72×10^{-5}	7.72×10^{-5}	100.0	5.6
Standard deviation		$=1.47\times10^{-4}$		

evaluated by steady state chronoamperometry tests conducted at 0.7 V for 5,000 s. Fig. S6 shows a current versus time measurement plot for glucose oxidation. It was noted that during initial 6 minutes, current density decreased gradually due to presence of intermediate species and followed by stabilization. This process occurs because of the initial availability of active sites without any adsorbed intermediates. However, as reaction continues further, the degree of adsorption of intermediate species is based on active sites of catalysts, which further leads to oxidation of adsorbed intermediate species leaving faster from active sites [65]. Therefore, PF-MoO_3 has superior catalytic activity to defeat poisoning of catalyst and thus provides high current density and stability. High electro-catalytic activity and excellent stability of PF-MoO_3 is governed by advantageous synergic effect between PF and MoO_3 which may cause structure roughness with high surface area. Therefore, these observations suggest PF-MoO_3 is a better electro-catalyst.

CONCLUSIONS

We have developed an enzyme free glucose sensor based on PF-MoO_3 nanocomposite. Successful synthesis of PF-MoO_3 composites was carried out in swollen liquid crystal lamellar mesophase. Micro-sphere structured PF-MoO_3 modified GCE electrode was used as glucose sensor. The designed sensor of PF-MoO_3/GCE boosted the analytical sensitivity of glucose by yielding a low detection limit of 7.90×10^{-5} M and 7.05×10^{-5} M by CV and DPV, respectively. The developed sensor provides excellent stability and reproducibility along with high catalytic activity. A highly sensitive glucose sensor was obtained due to enhancement of synergic effect shown by PF-MoO_3. Moreover, the sensor was successfully employed to determine glucose in human urine sample, and also PF-MoO_3/GCE served as a highly selective even in the existence of interfering species. Therefore, the sensing performance of the modified sensor reveals excellent environmental and electrochemical stability. This implies that with these characteristic features, the electrode materials have a potential to fabricate magnificent glucose sensing devices and assuredly open doors towards low-cost and sensitive glucose sensors.

CONFLICT OF INTEREST

The authors declare no conflict of interest.

SUPPORTING INFORMATION

Additional information as noted in the text. This information is available via the Internet at http://www.springer.com/chemistry/journal/11814.

REFERENCES

1. Y. Zhang, Y. Ma, Y. Li, W. Zhu, Z. Wei, J. Sun, T. Li and J. Wang, *Appl. Surf. Sci*., **505**, 144636 (2020).
2. M. Christwardana, J. Ji, Y. Chung and Y. Kwon, *Korean J. Chem. Eng*., **34**, 2916 (2017).
3. G. Wang, X. He, L. Wang, A. Gu, Y. Huang, B. Fang, B. Geng and X. Zhang, *Microchim. Acta*, **180**, 161 (2013).
4. M. Li, L. Liu, Y. Xiong, X. Liu, A. Nsabimana, X. Bo and L. Guo, *Sens. Actuators B*, **207**, 614 (2015).
5. K. E. Toghill and R. G. Compton, *Int. J. Electrochem. Sci*., **5**, 1246 (2010).
6. Z. G. Zhu, L. Garcia-Gancedo, A. J. Flewitt, H. Q. Xie, F. Moussy and W. I. Milne, *Sensors*, **12**, 5996 (2012).
7. M. Pumera and A. Loo, *TrAC Trends in Anal. Chem*., **61**, 49 (2014).
8. S. Balendhran, S. Walia, H. Nili, J. Ou, S. Zhuiykov, R. B. Kaner, S. Sriram, M. Bhaskaran and K. Kalantar-zadeh, *Adv. Funct. Mater.*, **23**, 3952 (2013).
9. V. M. Reddy, B. Sravani, T. Łuczak, K. Mallikarjunad and G. Madhavi, *Colloids Surf. A: Physicochem. Eng. Aspects*, **608**, 125533 (2021).
10. L. Zhang, H. Li, Y. Ni, J. Li, K. Liao and G. Zhao, *Electrochem. Commun*., **11**, 812 (2009).
11. Y. Xue, B. Tian, M. Wang, T. Zhai, R. Li and L. Tan, *Colloids Surf. A: Physicochem. Eng. Aspects*, **591**, 124549 (2020).
12. F. Meng, W. Shi, Y. Sun, X. Zhu, G. Wua, C. Ruan, X. Liu and D. Ge, *Biosens. Bioelectron*., **42**, 141 (2013).
13. A. M. Azharudeen, R. Karthiga, M. Rajarajan and A. Suganthi, *Microchem. J*., **157**, 105006 (2020).
14. I. Shakir and M. Sarfraz, *Electrochim. Acta*, **147**, 380 (2014).
15. Y. Wang, Y. Zhu, Z. Xing and Y. Qian, *Int. J. Electrochem. Sci*., **8**, 9851 (2013).
16. D. Murugesan, K. Moulaee, G. Neri, N. Ponpandian and C. Viswanathan, *Nanotechnology*, **30**, 265501 (2019).
17. W. Lei, W. Si, Y. Xu, Z. Gu and Q. Hao, *Microchim. Acta*, **181**, 707 (2014).
18. L. Li, H. Qiu, Y. Wang, J. Jiang and F. Xu, *J. Rare Earths*, **26**, 558 (2008).
19. J. Mort, *Science*, **208**, 819 (1980).
20. L. Zhang, S. Yuan and X. Lu, *Microchim. Acta*, **181**, 365 (2014).
21. J. Xie, X. Yang, S. Zhou and D. Wang, *ACS Nano*., **5**, 9225 (2011).
22. A. Mehdinia, H. Khani and S. Mozaffari, *Microchim. Acta*, **181**, 89 (2014).
23. A. Mostafaei and F. Nasirpouri, *Prog. Org. Coat*., **77**, 146 (2014).
24. F. Jiang, W. Li, R. Zou, Q. Liu, K. Xu, L. An and J. Hu, *Nano Energy*, **7**, 72 (2014).
25. S. Li, D. Wu, C. Cheng, J. Wang, F. Zhang, Y. Su and X. Feng, *Chem. Int. Ed*., **52**, 12105 (2013).
26. D. Neher, *Macromol. Electroluminescence Rap. Commun*., **22**, 1365 (2001).
27. U. Scherf and E. J. W List, *Adv. Mater*., **14**, 477 (2002).
28. G. Surendran, M. Tokumoto, E. Pena dos Santos, H. Remita, L. Ramos, P. Kooyman and J. Prouzet, *Chem. Mater*., **17**, 1505 (2005).
29. A. Tawade, D. Mohan kumar, P. Talele, K. K. Sharma and S. Tayade, *J. Electronic Mater*., **48**, 7747 (2019).
30. A. Chithambararaj and A. Bose, *J. Nanotechnol*., **2**, 585 (2011).
31. A. Aljabali, J. Barclay, J. George, B. Lomonossoffa and P. Evans, *Dalton Trans*., **39**, 7569 (2010).
32. G. S. Zakharova, C. Schmidt, A. Ottmann, E. Mijowska and R. Klingeler, *J. Solid State Electrochem*., **22**, 3651 (2018).
33. G. Farial, T. Plivelic, R. Cossiello and A. Multitechnique, *J. Phys. Chem. B*, **113**, 11403 (2009).
34. M. Jumali, B. Al-Asbahi. C. Yap, M. Salleh and M. Alsalhi, *Thin Solid Films*, **524**, 257 (2012).

35. T. Mika, G. Frank and S. Ullrich, *Macromolecules*, **48**, 5244 (2015).
36. M. Sims, D. D. C Bradely, M. Ariu, M. Koeberg, A. Asimakis, M. Grell and D. G. Lidzey, *Adv. Funct. Mater.*, **14**, 765 (2004).
37. K. Li, J. Pan, S. Feng, A. Wenqing, K. Pu, Y. Liu and B. Liu, *Adv. Funct. Mater.*, **19**, 3535 (2009).
38. S. E. Dhanavel, A. K. Nivethaa, K. Dhanapal, V. K. Gupta, V. Narayanan and A. Stephena, *RSC Adv.*, **6**, 28871 (2016).
39. B. A. Rozenberg and R. Tenne, *Prog. Polym. Sci.*, **33**, 40 (2008).
40. A. Chithambararaj and A. Bose, *J. Alloys Compd.*, **509**, 8105 (2011).
41. W. Zhao, T. Cao and J. M. White, *Adv. Funct. Mater.*, **14**, 783 (2004).
42. T. Marimuthu, S. Mohamad and Y. Alias, *Synthetic Metals*, **207**, 35 (2015).
43. B. Kamble, M. Naikwade, K. Garadkar, R. Mane, K. Sharma, B. Ajalkar and S. Tayade, *J. Mater. Sci.: Mater. Electron.*, **30**, 13984 (2019).
44. X. Li and X. Du, *Sens. Actuators B: Chem.*, **239**, 536 (2017).
45. K. Anderson, B. Poulter, J. Dudgeon, S.-E. Li and X. Ma, *Sensors*, **17**, 1807 (2017).
46. A. M. Azharudeen, R. Karthiga, M. Rajarajan and A. Suganthi, *Microchem. J.*, **157**, 105006 (2020).
47. M. Sharma, A. Gangan, B. Chakraborty and C. S. Rout, *J. Phys. D: Appl. Phys.*, **50**, 475401 (2017).
48. Y. J. Zhai, J. H. Li, X. Y. Chu, M. Z. Xu, F. J. Jin, X. Li, X. Fang, Z. P. Wei and X. H Wang, *J. Alloys Compd.*, **672**, 600 (2016).
49. P. Kannan, F. Chen, H. Jiang, H. Wang, R. Wang, P. Subramanian and S. Ji, *Analyst*, **144**, 4925 (2019).
50. H. Ren, L. Yan, M. Liu, Y. Wang, X. Liu, C. Liu, K. Liu, L. Zeng and A. Liu, *Sens. Actuators B: Chem.*, **296**, 126517 (2019).
51. L. Fang, F. Wang, Z. Chen, Y. Qiu, T. Zhai, M. Hu, C. Zhang and K. Huang, *Talanta*, **167**, 593 (2017).
52. Z. Zhang, D. Vieira, J. E. Barralet and G. Merle, *2D Mater.*, **7**, 025044 (2020).
53. Z. Shahnavaz, F. Lorestani, Y. Alias and P. M. Woi, *Appl. Surf. Sci.*, **317**, 622 (2014).
54. M. Lyons and G. P. Keeley, *Chem. Commun.*, **22**, 2529 (2008).
55. N. Hui, S. Wang, H. Xie, S. Xu, S. Niu and X. Luo, *Sens. Actuators B*, **221**, 606 (2015).
56. A. S. Kumar, P. Y. Chen, S. H. Chien and J. M. Zen, *Electroanalysis*, **3**, 17 (2005).
57. S. Park, H. Boo and T. Dong, *Anal. Chim. Acta*, **556**, 46 (2006).
58. F. Largeaud, K. B. Kokoh, B. Beden and C. J. Lamy, *Electroanal. Chem.*, **397**, 261 (1995).
59. S. Ernst, J. Heitbaum, C. H. Hamann and B. Bunsenges, *Phys. Chem.*, **84**, 50 (1980).
60. N. Hareesha and J. G. Manjunatha, *J. Iran Chem. Soc.*, **17**, 1507 (2020).
61. A. Bard and L. Faulkner, *Electrochemical methods: fundamentals and applications*, 2nd Edition, John Wiley, New York (2001).
62. B. B. Kamble, A. K. Tawade, P. Kamble, M. N. Padavi, K. K. Sharma, B. D. Ajalkar and S. N. Tayade, *Russian J. Electrochem.*, **56**, 766 (2020).
63. A. Raziq, M. Tariq, R. Hussian, M. Mehmood, M. S. Khan and A. Hassan, *Chem. Select.*, **2**, 9711 (2017).
64. B. B. Kamble, B. D. Ajalkar, A. K. Tawade, K. K. Sharma, S. S. Mali, C. K. Hong, C. Bathula, A. N. Kadam and S. N. Tayade, *J. Mol. Liq.*, **324**, 115119 (2021).
65. P. Mukherjee, P. S. Roy and S. K. Bhattacharya, *Int. J. Hydrogen Energy*, **40**, 13357 (2015).

Supporting Information

In situ soft templated synthesis of polyfluorene-molybdenum oxide (PF-MoO_3) nanocomposite: A nanostructure glucose sensor

Bhagyashri Bajirao Kamble*, Paurnima Talele, Anita Kundlik Tawade***, Kirankumar Kakchingtabam Sharma***, Sawanta Subhash Mali****, Chang Kook Hong****, and Shivaji Nemchand Tayade*,†**

*Department of Chemistry, Shivaji University, Kolhapur-416004, Maharashtra, India
**Department of Chemistry, Indian Institute of Technology Madras, Chennai-600036, India
***School of Nanoscience and Technology, Shivaji University, Kolhapur-416004, Maharashtra, India
****Polymer Energy Materials Laboratory, School of Advance Chemical Engineering,
Chonnam National University 61186, Korea
(*Received 20 August 2021 • Revised 8 November 2021 • Accepted 10 November 2021*)

Table S1. Comparatives outputs of the modified electrode used in the Glucose determination

Methods	Modified Electrodes	Sensitivity ($\mu Acm^{-2}\ mM^{-1}$)	Linear range (M)	LOD (M)	Reference
Amperometry	Au-Pd/MoS_2/GCE a	-	5×10^{-4} to 2×10^{-2}	4×10^{-4}	[44]
SWV	GC/Colloidal AgNPs/MoS_2	9,044.6	1×10^{-7} to 1×10^{-3}	3×10^{-8}	[45]
CV	MoO_3/PVP/GCE	86.42	up to 1×10^{-4}	2.20×10^{-8}	[46]
Amperometry	MoO_3	15.4 7.5	5×10^{-3}-1.75×10^{-1} 1.75×10^{-1} 6.15×10^{-1}	5.10×10^{-5} 1.04×10^{-4}	[47]
CV	MoS_2/NF	570.71	0-30	-	[48]
Amperometry	Ni_3S_2/$NiMoO_4$	10.49	0 to 2.40×10^{-4}	5.50×10^{-8}	[49]
Colorimetric	MoO_3/C nanorods	-	1×10^{-6} to 1×10^{-4}	1×10^{-5}	[50]
Amperometry	Cu_2O/MoS_2	3,108.08	1×10^{-5}-4×10^{-3}	1×10^{-6}	[51]
CV	PF-MoO_3/GCE	4.29×10^{4}	1.39×10^{-4} to 9. 72×10^{-4}	7.90×10^{-5}	This work
DPV	PF-MoO_3/GCE	5.18×10^{3}	2.77×10^{-4} to 9.72×10^{-4}	7.05×10^{-5}	This work

Effect of Scan Rate

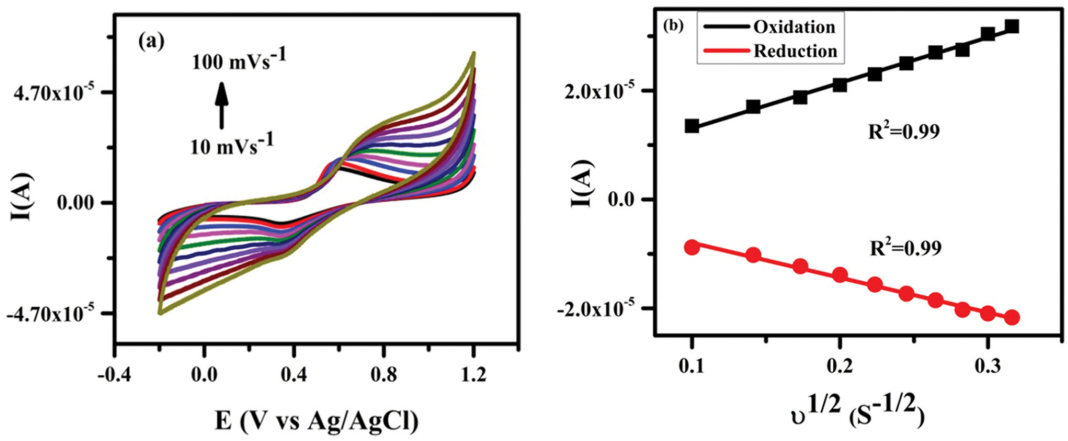

Fig. S1. (a) Cyclic voltammogram of (9.72×10^{-4} M) glucose at the PF-MoO_3/GCE (acetate buffer of 0.1 M; pH 7.4) at diverse scan rate (10 mVs^{-1} to 100 mVs^{-1}). (b) Dependance of redox peak current I (A) with respect to the square root of scan rate.

Electrochemical Impedance Spectroscopic (EIS) Studies

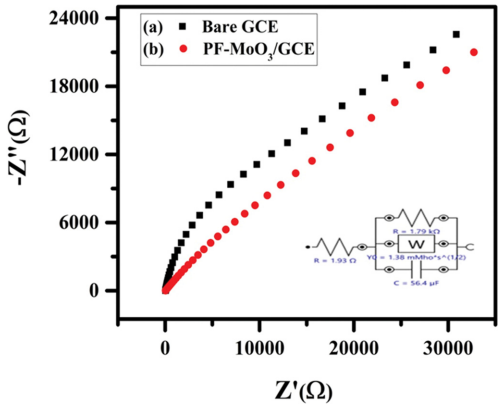

Fig. S2. Nyquist plot obtained for the electrodes (a) Bare GCE (b) PF-MoO_3/GCE in 1 mM ferrocene (inset figure represents circuit used in fitting EIS data for PF-MoO_3/GCE).

Chronoamperometric Study

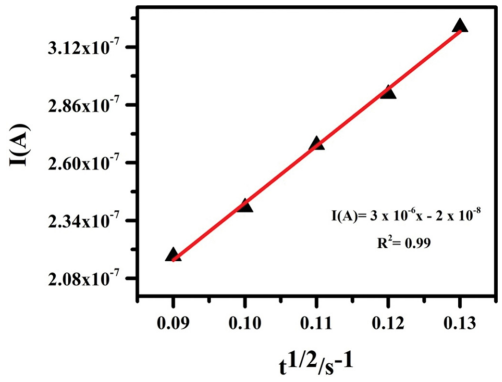

Fig. S3. Cottrell plot of $t^{1/2}$ Vs I(A) of 1 mM of glucose in 0.1 M acetate buffer solution (pH 7.4).

Interference Study of Biomolecules

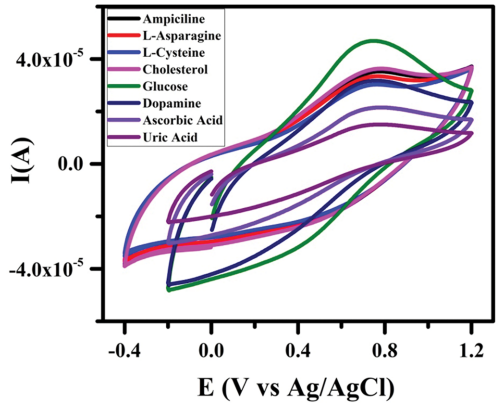

Fig. S4. The plot of anodic peak current Vs. Interfering species (DA, AA and UA) at PF-MoO_3/GCE in 0.1 M acetate buffer (pH 7.4).

Determination of Glucose in Human Urine Sample

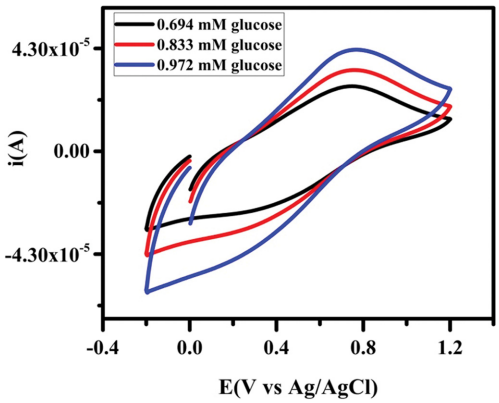

Fig. S5. Cyclic voltammogram of 0.694 mM, 0.833 mM and 0.972 mM glucose added in urine sample at PF-MoO_3/GCE in 0.1 M acetate buffer (pH 7.4).

Chronoamperometry Studies for Stability and Electro-catalytic Activity

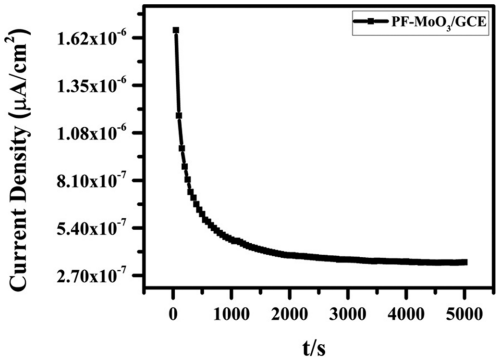

Fig. S6. Chronoamperometry at 0.7 V for PF-MoO_3/GCE in presence of 2.78×10^{-4} M of glucose in 0.1 M acetate buffer (pH 7.4).